pectations for a second-row transition-metal complex.[29] Finally, our pellet spectrum of $Cs_2[Mo_2(HPO_4)_4]\cdot 2H_2O$ showed a very intense absorption maximum at 250 nm. We consider it most unlikely that intense charge-transfer transitions involving the bridging phosphate or axial water ligands would occur at this low an energy and thus tentatively suggest that this band be assigned to the $^1(\pi \rightarrow \pi^*)(Mo_2)$ transition. Comparable UV data for the analogous sulfate complexes, however, have not yet been reported.

(29) An alternative assignment for the 670-nm band is $^1(\sigma(Mo_2) \rightarrow \delta(Mo_2))$ ($^1B_{2g} \leftarrow {}^1A_{1g}$; dipole-forbidden); recent photoelectron spectroscopic studies of other triply metal-metal bonded complexes indicate that the σ and π molecular orbitals of these species are nearly degenerate (Kober, E. M.; Lichtenberger, D. L. *J. Am. Chem. Soc.* **1985**, *107*, 7199-7201).

Acknowledgment. We thank W. H. Woodruff and W. P. Schaefer for assistance with the Raman spectroscopy and X-ray photography, respectively, and A. Bino for helpful discussions regarding the preparation of $Mo_2(HPO_4)_4^{2-}$. M.D.H. acknowledges the Sun Co. and Standard Oil Co. (Ohio) for graduate fellowships. This work was supported by National Science Foundation Grant CHE84-19828 (H.B.G.) and the Caltech President's Fund (V.M.M.).

Registry No. $(pyH)_3[Mo_2(HPO_4)_4]Cl$, 71597-13-2; $Cs_2[Mo_2(HPO_4)_4]\cdot 2H_2O$, 70281-26-4; $Mo_2(SO_4)_4^{4-}$, 63313-38-2; $Mo_2(HPO_4)_4^{2-}$, 75365-59-2.

Mixed-Valence 1′,6′-Dihalobiferrocenium Salts: The Effect of the Solid-State Environment on Electron-Transfer Rates

Teng-Yuan Dong,[1] David N. Hendrickson,*[1] Cortlandt G. Pierpont,*[2] and Michael F. Moore[1]

Contribution from the School of Chemical Sciences, University of Illinois, Urbana, Illinois 61801, and the Department of Chemistry, University of Colorado, Boulder, Colorado 80309. *Received July 23, 1985*

Abstract: Results for the room-temperature X-ray structures of mixed-valence 1′,6′-diiodobiferrocenium triiodide (**2**) and mixed-valence 1′,6′-dichlorobiferrocenium octaiodide(2-) (**4**) are reported. An interesting observation was made: the mixed-valence cation in **4** is valence localized with Fe^{II} and Fe^{III} ions, whereas, the cation in **2** has two crystallographically equivalent iron ions. In the case of **2** the structure was refined to give discrepancy factors of $R_F = 0.033$ and $R_{wF} = 0.038$ for 946 observed ($|F| > 6\sigma|F|$) reflections. Compound **2** crystallizes in the monoclinic space group $C2/m$ with two formula weights in a cell having the dimensions $a = 12.282$ (2) Å, $b = 8.935$ (1) Å, $c = 12.287$ (2) Å, and $\beta = 61.89$ (1)°. The mixed-valence 1′,6′-diiodobiferrocenium cation lies on a crystallographic mirror plane and is located about a twofold axis in the unit cell, imposing $2/m$ symmetry (trans conformation) on the cation. The packing arrangement in **2** consists of planar layers of cations and anions that are arranged in an alternating fashion on the crystallographic *ac* mirror plane. In the case of **4** the X-ray structure was refined to give discrepancy factors of $R_F = 0.064$ and $R_{wF} = 0.068$ for 1084 observed ($|F| > 6\sigma|F|$) reflections. Compound **4** crystallizes in the monoclinic space group $I2$ with four formula weights in a cell having the dimensions $a = 13.709$ (2) Å, $b = 14.189$ (2) Å, $c = 14.409$ (2) Å, and $\beta = 116.64$ (2)°. No crystallographic symmetry is imposed on the mixed-valence 1′,6′-dichlorobiferrocenium cation, although it does have the same trans conformation as found for the 1′,6′-diiodobiferrocenium cation. In marked contrast to the cation in **2**, for the 1′,6′-dichlorobiferrocenium cation one-half of the molecule has the dimensions of a Fe^{II} metallocene and the other half those of a Fe^{III} metallocene. In **4** the solid-state environments of the two iron ions in one cation are quite different due to the positioning of the I_3^- counterion, whereas, the anion in **2** is positioned symmetrically relative to the two iron ions in the cation. Variable-temperature ^{57}Fe Mössbauer, EPR, and IR data are presented for **2**, **4**, and 1′,6′-dibromobiferrocenium triiodide (**3**). Compound **4** gives a Mössbauer spectrum with two quadrupole-split doublets at 4.2 K; two doublets are also seen in the 340 K spectrum. On the other hand, compounds **2** and **3** give Mössbauer spectra with a single "average-valence" quadrupole-split doublet at 300 K. Furthermore, a single doublet is seen at 4.2 K for **2** and **3**. Compounds **2** and **3** exhibit relatively isotropic **g** tensors compared to **4**, as deduced from X-band EPR spectra. Compounds **2** and **3** are judged to have an intramolecular electron-transfer rate in excess of the Mössbauer and EPR time scales (rate $> \sim 10^{10}$ s^{-1}), whereas, the electron-transfer rate for **4** is slower than $\sim 10^7$ s^{-1}. However, all three compounds are found to be localized on the infrared time scale. It is concluded that it is *not* a variation in the electronic coupling between iron ions nor the vibronic coupling that leads to the appreciable change in electron-transfer rate that occurs in going from the dichloro cation to the two others. The differences in rates are attributable to differences in the symmetry of the solid-state environment.

Recent results obtained for the mixed-valence biferrocenes **1-8** have given insight about the influence of the solid-state environment on the rate of intramolecular electron transfer. Very recently the X-ray structures of **1**[3,4] and **7**[4] were reported. Previously compound **1** had been reported[5] to be localized on the Mössbauer time scale at 300 K. However, recently it was found[3,4] that at temperatures above 300 K the ^{57}Fe Mössbauer spectrum of **1** changes from two doublets to eventually become a single average-valence doublet at ~357 K. Mixed-valence compounds **5**,[6] **6**,[6] **7**,[4] and **8**[4] were also found to have temperature-dependent Mössbauer spectra. At temperatures below ~200 K they each show two doublets, one for the Fe^{II} and the other for the Fe^{III} site. As the temperature of these four compounds is increased above ~200 K the two doublets move together to become a single

(1) University of Illinois.
(2) University of Colorado.
(3) Cohn, M. J.; Dong, T.-Y.; Hendrickson, D. N.; Geib, S. J.; Rheingold, A. L. *J. Chem. Soc., Chem. Commun.* **1985**, *1095*.
(4) Dong, T.-Y.; Hendrickson, D. N.; Iwai, K.; Cohn, M. J.; Rheingold, A. L.; Sano, H.; Motoyama, I.; Nakashima, S. *J. Am. Chem. Soc.* **1985**, *107*, 7996.
(5) Morrison, W. H., Jr.; Hendrickson, D. N. *Inorg. Chem.* **1975**, *14*, 2331.
(6) Iijima, S.; Saida, R.; Motoyama, I.; Sano, H. *Bull. Chem. Soc. Jpn.* **1981**, *54*, 1375.

0002-7863/86/1508-0963$01.50/0

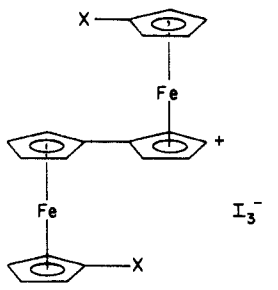

1, X = H 5, X = CH_2CH_3
2, X = I 6, X = $CH_2CH_2CH_3$
3, X = Br 7, X = $CH_2CH_2CH_2CH_3$
4, X = Cl 8, X = $CH_2(c\text{-}C_6H_5)$

average-valence doublet at temperatures of 275, 245, 275, and 260 K, respectively.

From single-crystal X-ray work it is known that the mixed-valence cations in **1**,[3,4] **6**,[8] and **7**[4] all have the trans conformation pictured with a planar fulvenide ligand. X-ray structural results presented in this paper show that the cations in **2**[7] and **4** also have the same trans conformation. Furthermore, compounds **8** and **5** are isostructural with **6**. Thus, it is likely that neither the electronic coupling (ϵ in the PKS theory[9]) nor the vibronic coupling (λ) is varying appreciably from one cation to another in the above series. In previous papers[3,4,7] we suggested that it is the environment about the mixed-valence cation in the solid state that controls whether and at what temperature *intra*molecular electron transfer occurs. The temperature dependence seen in the Mössbauer spectra of **1**, **5**, **6**, **7**, and **8** has been attributed[4] to dynamics in the solid state. The conversion that is occurring is from a static solid-state structure to a dynamical one. It is the onset of vibrational motion involving the I_3^- counterion that controls the rate of *intra*molecular electron transfer in the mixed-valence cation. When the I_3^- counterion is thermally activated, it interconverts between the two limiting forms $(I_A\cdots I_B—I_C)^-$ and $(I_A—I_B\cdots I_C)^-$. In each of these limiting forms the two iodine–iodine bond lengths are not equal. In effect, the I_3^- counterion is a mixed-valence species and the oscillatory charge motion associated with it controls whether charge can be pulled back and forth in the mixed-valence cation.

As will be shown in this paper, it is with compounds **2**, **3**, and **4** that we see the maximum influence of the solid-state environment on the rate of the *intra*molecular electron transfer in the cation. The cation in **4** is localized at 300 K on the Mössbauer time scale,[10] which means that the rate of electron transfer is less than $\sim 10^7$ s^{-1} at 300 K. On the other hand, the cations in **2** and **3** are transferring electrons faster than both the Mössbauer and EPR time scales not only at 300 K but also at 4.2 K.[5,10] This has been interpreted to mean that the intramolecular electron transfer for these two cations is faster than $\sim 10^{10}$ s^{-1} even at 4.2 K. The results of the X-ray structural work for **2** and **4**, together with variable-temperature ^{57}Fe Mössbauer, EPR, and IR data, are presented in this paper in an attempt to explain why the rate of electron transfer for **2** and **3** is at least three orders of magnitude faster than that in **4**.

Experimental Section

Compound Preparation. Samples of 1′,6′-diiodobiferrocene, 1′,6′-dibromobiferrocene, and 1′,6′-dichlorobiferrocene were prepared according to literature methods[11] and identified by melting point, ^{1}H NMR, and mass spectral data.

Samples of the mixed-valence compounds **2**, **3**, and **4** were prepared according to the simple procedure previously reported[5] for biferrocenium triiodide. Anal. Calcd for 1′,6′-diiodobiferrocenium triiodide ($C_{20}H_{16}Fe_2I_5$): C, 23.96; H, 1.16; Fe, 11.14; I, 63.29. Found: C, 24.15; H, 1.69; Fe, 11.27; I, 63.37. Calcd for 1′,6′-dibromobiferrocenium triiodide ($C_{20}H_{16}Fe_2Br_2I_3$): C, 26.44; H, 1.78; Fe, 12.29; Br, 17.59; I, 41.90. Found: C, 27.02; H, 1.95; Fe, 12.73. Calcd for 1′,6′-dichlorobiferrocenium octaiodide(2−) ($C_{20}H_{16}Fe_2Cl_2I_4$): C, 25.38; H, 1.70; Fe, 11.80; I, 53.63. Found: C, 25.76; H, 1.94; Fe, 12.25; I, 54.30.

Crystals of 1′,6′-dichlorobiferrocenium octaiodide(2−) and 1′,6′-diiodobiferrocenium triiodide were grown by diffusing a hexane solution containing a stoichiometric amount of I_2 into a CH_2Cl_2 solution containing the 1′,6′-disubstituted biferrocene.

Physical Methods. ^{57}Fe Mössbauer measurements were made on a constant-velocity-type instrument which has been described previously.[12] We estimate the absolute temperature accuracy to be ±3 K; the relative precision is ±0.5 K. Mössbauer spectra were least-squares fit to Lorentzian line shapes with a previously documented computer program.[13] Isomer shift data are reported relative to that of iron foil at 298 K but are not corrected for temperature-dependent second-order Doppler effects. It should be noted that the isomer shifts illustrated in the figures are plotted as experimentally obtained.

X-band EPR spectra of powdered samples were run on a Bruker ER200 spectrometer equipped with an Oxford Instruments temperature controller. A calibrated copper–constantan thermocouple was used to determine the sample temperature.

Infrared spectra were obtained with Nicolet Model MX-5 FT spectrometer. All samples were prepared as 13 mm KBr pellets with 2–5 mg of compound mixed well with 150 mg of KBr. A Spectrim closed-cycle refrigerator (Cryogenic Technology, Inc.) was used to cool the KBr pellets to ~50 K. The temperature of the KBr-pellet holder was monitored with an iron-doped gold thermocouple.

Structure Determination of $[(IC_5H_4Fe)_2(C_{10}H_8)]I_3$. Details of the structure determination of 1′,6′-diiodobiferrocenium triiodide are given in Table I. The structure was solved by using direct methods. Standard reflections monitored during data collection showed no significant deviations from their average values. The greatest residual electron density upon completion of refinement was in the region of the triiodide ion. During the final cycles of refinement fixed hydrogen contributions with C–H bond lengths fixed at 0.98 Å were applied for the ring hydrogen atoms. Final positional and thermal parameters for the structure are given in Table II.

Structure Determination on $[(ClC_5H_4Fe)_2(C_{10}H_8)]I_3 \cdot 0.5I_2$. Crystals of 1′,6′-dichlorobiferrocenium octaiodide form as flat plates. Large crystals of the complex tend to be laminar stacks of planar crystals. The crystal selected for data collection was less than ideal, but it was the best of the single crystals available. It was mounted so as to minimize the absorption effect, and due to its weak diffraction, data were collected to 2θ of 45°. Statistics on the data indicated that the unit cell was acentric and Patterson peaks were consistent with space group *I*2. The structure was solved by using a combination of direct methods and Patterson solutions. Standard reflections showed a linear decrease in intensity of 12% during data collection and data were corrected for this decrease. Crystal data and parameters used in the structure determination are given in Table III. Final positional and thermal parameters for the structure are given in Table IV. As before, fixed contributions for hydrogen atoms were included, and the largest peaks of residual electron density were located in the vicinity of the iodide atoms. Once the refinement had converged additional cycles of refinement were carried out with inverted atomic coordinates. The discrepancy index decreased by 0.1%, and the agreement between C–Cl and C–C bond lengths within the cation improved. This was judged to be the correct polarity for the atom coordinates of the structure.

Anisotropic thermal parameters and tables of structure factors for both structures are available in the supplementary material.

Results and Discussion

X-ray Structure of 1′,6′-Diiodobiferrocenium Triiodide. The results of our crystallographic study at 295 K show that the mixed-valence compound **2** crystallizes in the monoclinic space group *C*2/*m*. The 1′,6′-diiodobiferrocenium cation lies on a crystallographic mirror plane and is located about a twofold axis in the unit cell imposing 2/m symmetry (trans conformation) on the cation. Iodine ring substituents are in a trans conformation and are required by symmetry to lie on the mirror plane. A perspective drawing of the cation is shown in Figure 1 and selected bond distances and angles are given in Table V. Average distances

(7) The X-ray structure of **2** has been communicated: Dong, T.-Y.; Cohn, M. J.; Hendrickson, D. N.; Pierpont, C. G. *J. Am. Chem. Soc.* **1985**, *107*, 4777.
(8) Konno, M.; Hyodo, S.; Iijima, S. *Bull. Chem. Soc. Jpn.* **1982**, *55*, 2327.
(9) Wong, K. Y.; Schatz, P. N. *Prog. Inorg. Chem.* **1981**, *28*, 369.
(10) Motoyama, I.; Suto, K.; Katada, M.; Sano, H. *Chem. Lett.* **1983**, 1215.
(11) Kovar, R. F.; Rausch, M. D.; Rosenberg, H. *Organomet. Chem. Synth.* **1971**, *1*, 173.
(12) Cohn, M. J.; Timken, M. D.; Hendrickson, D. N. *J. Am. Chem. Soc.* **1984**, *106*, 6683.
(13) Chrisman, B. L.; Tumolillo, T. A. *Comput. Phys. Commun.* **1971**, *2*, 322.

Table I. Crystal Data and Details of the Structure Determination for $[(IC_5H_4Fe)_2(C_{10}H_8)]I_3$

Crystal Data	
formula	$Fe_2I_5C_{20}H_{16}$
mol wt	1002.5
space group[a]	$C2/m$
crystal system	monoclinic
a, Å	12.282 (2)
b, Å	8.935 (1)
c, Å	12.287 (2)
α, deg	90.00
β, deg	61.89 (1)
γ, deg	90.00
volume, Å^3	1189.3 (3)
z	2
d_{calcd}, g cm^{-3}	2.799
$F(000)$	800
μ, cm^{-1}	63.63
crystal dimensions, mm	0.42 × 0.21 × 0.11
Data Collection and Reduction	
diffractometer	Syntex P$\bar{1}$
data collected	$+h,+k,+l$; $+h,+k,-l$
radiation, Å	Mo Kα (0.71069)
monochromator angle, deg	12.2
temperature, K	294–296
scan technique	θ–2θ
scan range (2θ), min – max	3.0–50.0
scan speed, deg/min	4.0
scan range	0.7° below Kα_1, and 0.7° above Kα_2
background	stationary crystal–stationary counter; background time = 0.5 (scan time)
no. of unique reflections measured	2094
no. of obsd reflections criterion	946 $F > 6\sigma(F)$
absorption correction	empirical
transmission factors	0.99–0.58
Structure Determination and Refinement	
programs used	SHELX[c]
scattering factors	neutral atoms[d]
R_1 and R_2	0.033, 0.038
weight	$1/(\sigma(F)^2 + 0.0005F^2)$
no. of parameters	71
ratio of observations to parameters	13.3
maximum shift/error (non-hydrogen)	0.021
residual electron density, e$^-$/Å^3	2.1

[a] "International Tables for X-ray Crystallography", Kynoch Press: Birmingham, England, 1965; Vol. 1. [b] Cell dimensions were determined by least-squares fit of the setting angles of 15 reflections with 2θ in the range 20–30°. [c] G. M. Sheldrick, SHELX76, A Program for Crystal Structure Determination, University of Cambridge, England. [d] "International Tables for X-ray Crystallography", Kynoch Press: Birmingham, England, 1974; pp 55–60, 99–101, 149–150. [e] The quantity minimized in the least-squares procedures is $\sum w(|F_o| - |F_c|)^2$. $R_1 = \sum||F_o| - |F_c||/\sum|F_o|$. $R_2 = [\sum w(|F_o| - |F_c|)^2/\sum w(F_o)^2]^{1/2}$.

Table II. Positional and Thermal Parameters for $[(IC_5H_4Fe)_2(C_{10}H_8)]I_3$

atom	x	y	z	U[a]
I(1)	0.16931 (6)	0	0.51643 (7)	0.0485 (4)
I(2)	0	0	0	0.0393 (5)
I(3)	0.12534 (9)	0	0.15145 (8)	0.0714 (6)
Fe	0.5042 (1)	0	0.2895 (1)	0.0287 (7)
C(1)	0.5474 (8)	0	0.4349 (8)	0.034 (4)
C(2)	0.5952 (5)	0.1299 (8)	0.3600 (5)	0.035 (3)
C(3)	0.6791 (6)	0.0795 (8)	0.2380 (6)	0.039 (3)
C(4)	0.3172 (9)	0	0.3381 (9)	0.040 (5)
C(5)	0.3747 (7)	0.1306 (9)	0.2695 (6)	0.047 (4)
C(6)	0.4704 (7)	0.0803 (9)	0.1513 (6)	0.051 (5)

[a] Hamilton, W. C. *Acta Crystallogr.* **1959**, *12*, 609.

from the iron atoms to the ring carbon atoms are 2.070 (5) and 2.073 (5) Å to the iodocyclopentadienyl and fulvenide rings,

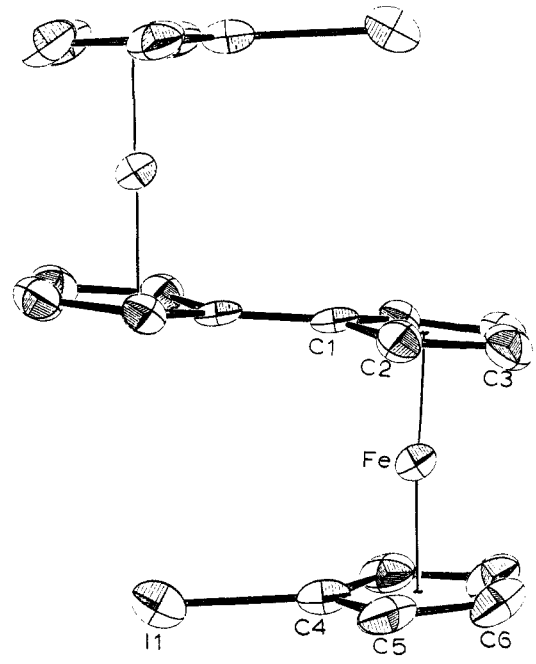

Figure 1. ORTEP plot showing the 1',6'-diiodobiferrocenium cation. The cation is located about a site of crystallographic $2/m$ symmetry.

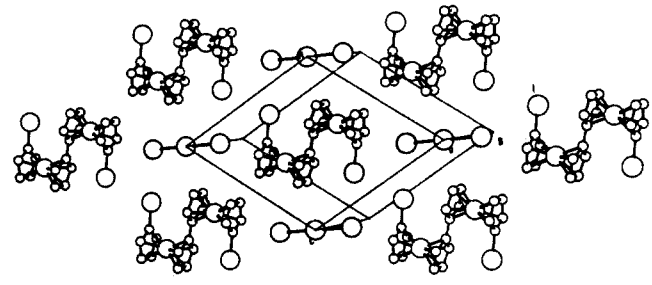

Figure 2. A PLUTO plot showing the arrangement of 1',6'-diiodobiferrocenium cations and triiodide anions on the crystallographic mirror plane of the unit cell. The separation between iodocyclopentadienyl iodine atoms and I_3^- ions in 3.98 Å.

respectively. These distances are closer to the value of 2.075 Å found[14] for the ferrocenium cation than the value of 2.045 Å found[15] for ferrocene. Distances from the iron to the centers-of-mass of the two rings are 1.672 and 1.676 Å, and the distance between centers of mass is 3.342 Å. The fulvenide ligand is required by site symmetry to be planar, and the planes of the iodocyclopentadienyl ligands form a dihedral angle of 15.6° with the fulvenide plane.

The triiodide anions in **2** are also located about sites of $2/m$ symmetry. The I_3^- anion has a I(2)–I(3) bond distance of 2.921 (1) Å. This corresponds well to the value of 2.920 Å reported[16] for the free I_3^- ion and is also close to the value of 2.926 (1) Å found[3,4] for biferrocenium triiodide.

The packing arrangement in **2** consists of planar layers of cations and anions that are arranged in an alternating fashion on the crystallographic *ac* mirror plane. A view of one plane is shown in Figure 2. The most significant interaction linking ions on this plane is between end iodine atoms of two I_3^- anions and two iodocyclopentadienyl iodine atoms. The I(1)–I(3) and I(1)–I(1') contacts are nonbonding and range from 3.98 to 4.36 Å. The closest cation–anion contact is between I(2) and the C(2) atoms of the fulvenide ring (3.70 Å).

The site symmetry imposed on the mixed-valence cation obviously requires that both iron centers of the cation residue in environmentally equivalent positions in the unit cell. An analysis of the thermal ellipsoids of ring carbon atoms indicates that this is not the result of a disordered localized structure.

X-ray Structure of 1',6'-Dichlorobiferrocenium Octaiodide(2–). In the acentric space group $I2$ no crystallographic symmetry is

III. Crystal Data and Details of the Structure Determination for $[(ClC_5H_4Fe)_2(C_{10}H_8)]I_3 \cdot 0.5I_2$

Crystal Data	
formula	$Fe_2I_4Cl_2C_{20}H_{16}$
mol wt	946.5
space group[a]	*I*2
crystal system	monoclinic
a, Å[b]	13.709 (2)
b, Å	14.189 (2)
c, Å	14.409 (2)
α, deg	90.00
β, deg	116.64 (2)
γ, deg	90.00
volume, Å^3	2505.1 (5)
z	4
d_{calcd}, g cm^{-3}	2.51
F(000)	1736
μ, cm^{-1}	62.61
crystal dimensions, mm	0.28 × 0.17 × 0.04
Data Collection and Reduction	
diffractometer	Syntex P$\bar{1}$
data collected	$+h,+k,+l$; $+h,+k,-l$
radiation, Å	Mo Kα (0.71069)
monochromator angle	12.2
temperature, K	294–296
scan technique	θ–2θ
scan range (2θ), min – max	3.0–45.0
scan speed, deg/min	4.0
scan range	0.7° below Kα_1 and 0.7° above Kα_2
background	stationary crystal–stationary counter; background time = 0.5 (scan time)
no. of unique reflections measured	1794
no. of obsd reflections	1084
criterion	$F > 6\sigma(F)$
absorption correction	empirical
transmission factors	0.99–0.74
Structure Determination and Refinement	
programs used	SHELX[c]
scattering factors	neutral atoms[d]
R_1 and R_2	0.064, 0.068
weight	$1/(\sigma(F)^2 + 0.0005F^2)$
no. of parameters	152
ratio of observations to parameters	7.1
max shift/error (non-hydrogen)	0.104
residual electron density, e$^-$/Å	3.3

[a] "International Tables for X-ray Crystallography"; Kynoch Press: Birmingham, England; Vol. 1, 1965. [b] Cell dimensions were determined by least-squares fit of the setting angles of 15 reflections with 2θ in the range 15–25°. [c] G. M. Sheldrick, SHELX76, A Program for Crystal Structure Determination, University of Cambridge, England. [d] "International Tables for X-ray Crystallography"; Kynoch Press: Birmingham, England, 1974; Vol. 4 pp 55–60, 99–101, 149–150. [e] The quantity minimized in the least-squares procedures is $\sum w(|F_o| - |F_c|)^2$. $R_1 = \sum||F_o| - |F_c||/\sum|F_o|$. $R_2 = [\sum w(|F_o| - |F_c|)^2/\sum w(F_o)^2]^{1/2}$.

imposed on the 1′,6′-dichlorobiferrocenium cation. It has the same trans conformation found for the diiodo analogue, although, the C–Cl bonds are rotated 1.8° (C(11)) and 16.3° (C(12)) from positions directly over the bridging C–C bond of the fulvenide rings. Selected bond distances and angles for the cation and anion are given in Table VI. Iron–carbon lengths of the cation differ consistently for the two iron ions. The average Fe(1)–C lengths to the chlorocyclopentadienyl and fulvenide rings are 2.09 and 2.08 Å, respectively, and the corresponding lengths of Fe(2) are 2.05 and 2.02 Å. The average Fe–C length for all bonds of the structure, 2.06 Å, agrees well with the average Fe–C length of the 1′,6′-diiodobiferrocenium cation, 2.071 Å. Iron separations to ring centers-of-mass (COM) are both 1.69 Å for Fe(1) and 1.61 and 1.65 Å for Fe(2). At both metals the shortest separation is to the fulvenide ring. Ring COM to COM separations at the two metals are 3.38 Å for Fe(1) and 3.26 Å for Fe(2). Dihedral angles between chlorocyclopentadienyl and fulvenide rings at the two metals are 6.9° at Fe(1) and 5.0° at Fe(2), and the dihedral angle between the planes of the two fulvenide rings is 6.8°.

Table IV. Atomic Positional and Thermal Parameters for $[(ClC_5H_4Fe)_2(C_{10}H_8)]I_3 \cdot 0.5I_2$

atom	*x*	*y*	*z*	U^a
I(1)	−0.0986 (3)	−0.02	0.0057 (3)	0.069 (2)
I(2)	−0.3323 (3)	−0.0104 (4)	0.0319 (2)	0.065 (2)
I(3)	−0.4300 (3)	0.1503 (4)	−0.1164 (3)	0.068 (2)
I(4)	−0.5169 (3)	0.3018 (5)	−0.2600 (3)	0.082 (3)
Fe(1)	−0.1916 (5)	0.3467 (6)	0.1774 (5)	0.039 (4)
Fe(2)	0.1840 (5)	0.2057 (6)	0.2876 (4)	0.039 (4)
Cl(1)	−0.065 (1)	0.485 (2)	0.078 (1)	0.11 (1)
Cl(2)	0.077 (1)	0.111 (1)	0.435 (1)	0.16 (2)
C(1)	−0.180 (3)	0.461 (3)	0.092 (3)	0.05 (1)
C(2)	−0.270 (4)	0.401 (4)	0.026 (4)	0.07 (2)
C(3)	−0.346 (4)	0.397 (4)	0.073 (4)	0.08 (2)
C(4)	−0.306 (3)	0.454 (3)	0.159 (3)	0.05 (1)
C(5)	−0.199 (4)	0.494 (4)	0.173 (4)	0.07 (1)
C(6)	0.179 (3)	0.113 (3)	0.397 (3)	0.04 (1)
C(7)	0.185 (4)	0.068 (4)	0.321 (4)	0.06 (1)
C(8)	0.279 (4)	0.088 (4)	0.315 (4)	0.08 (2)
C(9)	0.343 (4)	0.167 (4)	0.391 (4)	0.07 (2)
C(10)	0.270 (4)	0.179 (3)	0.445 (3)	0.05 (1)
C(11)	−0.053 (3)	0.254 (3)	0.232 (3)	0.04 (1)
C(12)	−0.151 (4)	0.207 (4)	0.174 (4)	0.06 (1)
C(13)	−0.215 (4)	0.211 (4)	0.220 (4)	0.06 (1)
C(14)	−0.180 (4)	0.280 (3)	0.306 (3)	0.05 (1)
C(15)	−0.071 (4)	0.304 (4)	0.319 (3)	0.05 (1)
C(16)	0.043 (4)	0.282 (4)	0.217 (4)	0.05 (1)
C(17)	0.063 (3)	0.225 (3)	0.145 (3)	0.04 (1)
C(18)	0.168 (4)	0.260 (4)	0.150 (4)	0.07 (2)
C(19)	0.212 (3)	0.324 (4)	0.232 (3)	0.05 (1)
C(20)	0.132 (3)	0.344 (3)	0.270 (3)	0.04 (1)

[a] Hamilton, W. C. *Acta Crystallogr.* **1959**, *12*, 609.

V. Bond Distances and Angles for $[(IC_5H_4Fe)_2(C_{10}H_8)]I_3$

Interatomic Distances, Å			
I(1)–C(4)	2.086 (0.010)	I(2)–I(3)	2.921 (0.001)
Fe–C(1)	2.089 (0.007)	Fe–C(2)	2.063 (0.006)
Fe–C(3)	2.058 (0.006)	Fe–C(4)	2.083 (0.009)
Fe–C(5)	2.078 (0.007)	Fe–C(6)	2.058 (0.006)
C(1)–C(2)	1.425 (0.008)	C(1)–C(1)	1.470 (0.017)
C(2)–C(3)	1.434 (0.009)	C(3)–C(3)	1.421 (0.014)
C(4)–C(5)	1.417 (0.009)	C(5)–C(6)	1.443 (0.010)
C(6)–C(6′)	1.436 (0.016)		
Angles, deg			
C(2)–Fe–C(1)	40.1 (0.2)	C(3)–Fe–C(1)	67.3 (0.3)
C(3)–Fe–C(2)	40.7 (0.2)	C(4)–Fe–C(1)	116.4 (0.3)
C(4)–Fe–C(2)	128.4 (0.3)	C(4)–Fe–C(3)	159.7 (0.2)
C(5)–Fe–C(1)	128.2 (0.3)	C(5)–Fe–C(2)	109.2 (0.3)
C(5)–Fe–C(3)	121.0 (0.3)	C(5)–Fe–C(4)	39.8 (0.2)
C(6)–Fe–C(1)	159.5 (0.2)	C(6)–Fe–C(2)	120.6 (0.3)
C(6)–Fe–C(3)	102.3 (0.3)	C(6)–Fe–C(4)	67.2 (0.3)
C(6)–Fe–C(5)	40.8 (0.3)	C(2)–C(1)–Fe	69.0 (0.4)
C(1)–C(2)–Fe	70.9 (0.4)	C(3)–C(2)–Fe	69.5 (0.4)
C(3)–C(2)–C(1)	107.1 (0.6)	C(2)–C(3)–Fe	69.8 (0.3)
C(3)–Fe–C(3)	40.4 (0.4)	Fe–C(4)–I(1)	126.7 (0.4)
C(5)–C(4)–I(1)	124.6 (0.4)	C(5)–C(4)–Fe	69.9 (0.4)
C(4)–C(5)–Fe	70.3 (0.4)	C(6)–C(5)–Fe	68.8 (0.4)
C(6)–C(5)–C(4)	106.5 (0.7)	C(5)–C(6)–Fe	70.3 (0.3)
C(6)–Fe–C(6)	40.8 (0.4)		

Cocrystallized in the unit cell is an I_2 molecule located about a crystallographic twofold axis. Bonded to the I_2 atoms are the end atoms of the triiodide ion with an I(1)–I(2) length of 3.392 Å and a I(1)–I(1)–I(2) bond angle of 176.49°. With twofold symmetry, the result is an I_8^{2-} dianion, shown with two related complex cations in Figure 3. The dihedral angle between related I(1), I(2), I(3), I(4) planes is 81.4°.

The solid-state environments of the two iron ions in one cation are quite different due to the cation–anion relationship. The atom Fe(1) is closest to a linear arrangement of anion iodine atoms which is roughly parallel to the cyclopentadienyl rings, while Fe(2) is closest to a region of the anion extending in a direction which is approximately perpendicular to the ring planes. The shortest

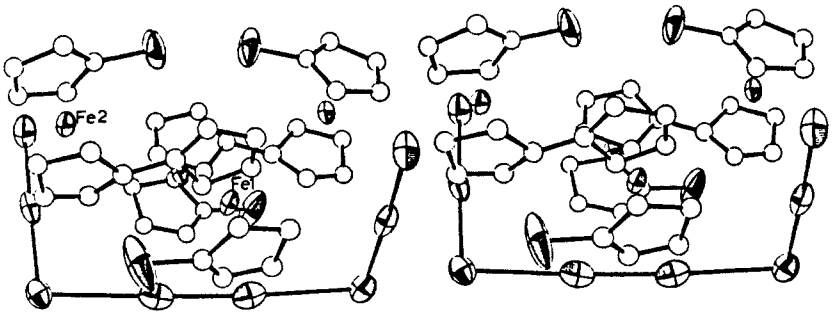

Figure 3. A stereoview showing the I_8^{2-} anion and two 1',6'-dichlorobiferrocenium cations related by a crystallographic twofold axis extending in the vertical direction of the figure.

VI. Bond Distances and Selected Bond Angles for $[(ClC_5H_4Fe)_2(C_{10}H_8)]I_3 \cdot 0.5I_2$

	Interatomic Distances, Å		
I(1)-I(2)	3.392 (0.005)	I(1)-I(1)	2.782 (0.008)
I(2)-I(3)	3.000 (0.006)	I(3)-I(4)	2.848 (0.006)
Fe(1)-C(1)	2.067 (0.047)	Fe(1)-C(2)	2.112 (0.053)
Fe(1)-C(3)	2.100 (0.056)	Fe(1)-C(4)	2.085 (0.044)
Fe(1)-C(5)	2.105 (0.062)	Fe(1)-C(11)	2.139 (0.043)
Fe(1)-C(12)	2.057 (0.051)	Fe(1)-C(13)	2.093 (0.053)
Fe(1)-C(14)	2.014 (0.045)	Fe(1)-C(15)	2.047 (0.042)
Fe(2)-C(6)	2.078 (0.043)	Fe(2)-C(7)	2.014 (0.053)
Fe(2)-C(8)	2.056 (0.060)	Fe(2)-C(9)	2.082 (0.051)
Fe(2)-C(10)	2.069 (0.044)	Fe(2)-C(16)	2.040 (0.045)
Fe(2)-C(17)	1.996 (0.040)	Fe(2)-C(18)	2.047 (0.054)
Fe(2)-C(19)	2.003 (0.048)	Fe(2)-C(20)	2.062 (0.043)
Cl(1)-C(1)	1.740 (0.047)	Cl(2)-C(6)	1.708 (0.043)
C(1)-C(2)	1.44 (0.06)	C(1)-C(5)	1.37 (0.05)
C(2)-C(3)	1.46 (0.07)	C(3)-C(4)	1.36 (0.06)
C(4)-C(5)	1.52 (0.05)	C(6)-C(7)	1.38 (0.05)
C(6)-C(10)	1.45 (0.05)	C(7)-C(8)	1.38 (0.06)
C(8)-C(9)	1.48 (0.07)	C(9)-C(10)	1.50 (0.06)
C(11)-C(12)	1.39 (0.05)	C(11)-C(15)	1.44 (0.05)
C(11)-C(16)	1.49 (0.05)	C(12)-C(13)	1.31 (0.05)
C(13)-C(14)	1.48 (0.06)	C(14)-C(15)	1.47 (0.05)
C(16)-C(17)	1.42 (0.05)	C(16)-C(20)	1.41 (0.05)
C(17)-C(18)	1.50 (0.06)	C(18)-C(19)	1.39 (0.06)
C(19)-C(20)	1.45 (0.05)		
	Selected Angles, deg		
I(3)-I(2)-I(1)	95.4 (0.1)	I(4)-I(3)-I(2)	177.9 (0.2)
C(2)-C(1)-Cl(1)	125 (3)	C(5)-C(1)-Cl(1)	123 (3)
C(5)-C(1)-C(2)	111 (4)	C(3)-C(2)-C(1)	106 (4)
C(4)-C(3)-C(2)	107 (4)	C(5)-C(4)-C(3)	109 (4)
C(4)-C(5)-C(1)	104 (4)	C(7)-C(6)-Cl(2)	128 (4)
C(10)-C(6)-Cl(2)	120 (3)	C(10)-C(6)-C(7)	111 (4)
C(8)-C(7)-C(6)	112 (5)	C(9)-C(8)-C(7)	108 (5)
C(10)-C(9)-C(8)	98 (4)	C(9)-C(10)-C(6)	108 (3)
C(15)-C(11)-C(12)	104 (3)	C(16)-C(11)-C(12)	135 (4)
C(16)-C(11)-C(15)	118 (4)	C(13)-C(12)-C(11)	111 (4)
C(14)-C(13)-C(12)	113 (4)	C(15)-C(14)-C(13)	100 (4)
C(14)-C(15)-C(11)	108 (3)	C(17)-C(16)-C(11)	115 (4)
C(20)-C(16)-C(11)	132 (4)	C(20)-C(16)-C(17)	110 (3)
C(18)-C(17)-C(16)	105 (4)	C(19)-C(18)-C(17)	108 (4)
C(20)-C(19)-C(18)	108 (3)	C(19)-C(20)-C(16)	107 (3)

cation–anion contact is between I(2) and C(14) with a value of 3.73 Å. It is this environmental dissimilarity which likely is responsible for the localized valence of the 1',6'-dichlorobiferrocenium cation.

^{57}Fe Mössbauer Characteristics. Mössbauer spectra were run at 300 and 4.2 K for compounds **2**, **3**, and **4**. As reported before,[10] the 1',6'-dichlorobiferrocenium cation in **4** is localized on the Mössbauer time scale at 4.2 K and remains localized up to 300 K. In order to see if **4** becomes "Mössbauer-delocalized" above 300 K as seen[3,4] for biferrocenium triiodide, a spectrum was run at 340 K. As can be seen in Figure 4, the 1',6'-dichlorobiferrocenium cation in **4** remains localized even up to 340 K. The cations in **2** and **3** have *intra*molecular electron-transfer rates that exceed $\sim 10^7$ s^{-1} not only at 300 K but also at 4.2 K. Thus, for compounds **2** and **3** only a single "average-valence" doublet is seen from 300 to 4.2 K. The 4.2 K spectra of **2** and **3** are illustrated in Figure 5. All of the spectra were least-squares fit with Lorentzian lineshapes; the resulting parameters are given in Table VII. It should be noted that the parameters given in Table VII differ slightly from those reported[5,10] previously. This results from the fact that the present spectra were run on a larger velocity range than before and this gives a more accurate representation of the spectral base line.

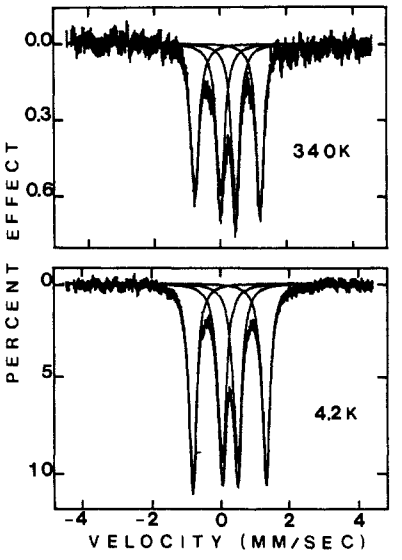

Figure 4. ^{57}Fe Mössbauer spectra of 1',6'-dichlorobiferrocenium octaiodide(2–), **4**.

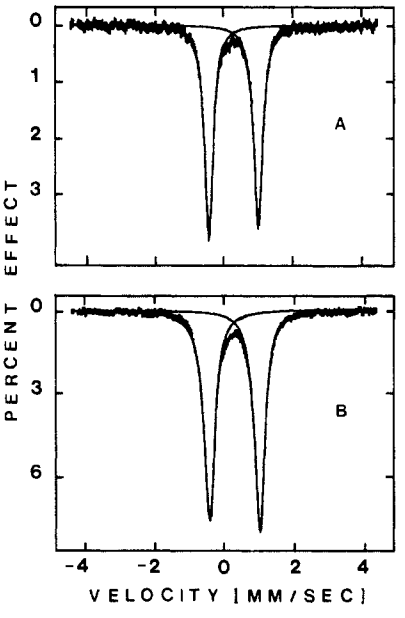

Figure 5. ^{57}Fe Mössbauer spectra at 4.2 K for (A) 1',6'-diiodobiferrocenium triiodide (**2**) and (B) 1',6'-dibromobiferrocenium triiodide (**3**).

Table VII. ^{57}Fe Mössbauer Fitting Parameters

compd	T, K	ΔE_Q	δ^b	Γ^c	
2	300	1.340 (2)	0.484 (1)	0.286 (3)	0.282 (3)
	4.2	1.438 (2)	0.514 (1)	0.292 (3)	0.308 (3)
3	300	1.314 (2)	0.482 (1)	0.294 (4)	0.290 (4)
	4.2	1.434 (1)	0.508 (1)	0.372 (2)	0.352 (2)
4	340	1.976 (6)	0.482 (3)	0.296 (11)	0.266 (10)
		0.450 (6)	0.504 (3)	0.298 (10)	0.278 (9)
	320	1.982 (5)	0.487 (3)	0.284 (10)	0.268 (9)
		0.452 (5)	0.508 (3)	0.322 (10)	0.312 (10)
	300	1.984 (4)	0.489 (2)	0.270 (7)	0.260 (7)
		0.450 (4)	0.492 (2)	0.310 (8)	0.296 (8)
	4.2	2.142 (2)	0.509 (1)	0.260 (4)	0.270 (4)
		0.451 (2)	0.521 (1)	0.290 (4)	0.288 (4)

[a] ΔE_Q and Γ values are given in units of mm/s; the estimated standard deviations in the least significant figures are given in parentheses. [b] Isomer shift relative to iron metal at room temperature. [c] Full width at half-height taken from the least-squares fitting program. The width for the line at more negative velocity is listed first for each doublet.

From Table VII and Figures 4 and 5 it is evident that the quadrupole splittings of the single doublets observed for **2** and **3** are, at either 300 or 4.2 K, close to the average of the quadrupole splittings for the two doublets of compound **4**. For example, at 4.2 K ΔE_Q is 1.438 (2) mm/s for the doublet of **2**, which is to be compared with an *average* of 1.296 (2) mm/s for the two doublets in the spectrum of **4**. The "average" values of ΔE_Q seen for **2** and **3** could indicate that there is only a weak or at most a moderate strength electronic coupling between the d-manifolds on the two iron ions in the cations of **2** and **3**. If the electronic coupling between the two iron ions in the cations of **2** and **3** was strong, there would be appreciable contributions from the fulvenide ligand to the molecular orbital in which the unpaired electron resides. The d orbitals on the two iron ions would become admixed with orbitals from the "bridging" fulvenide ligand. The greater the admixture the greater the probability for unpaired electron density on the fulvenide. Under this circumstance the iron ions lose to some degree their "Fe^{III} character", and this loss results in an increase in ΔE_Q because each iron ion is closer to Fe^{II} in its properties. This is what apparently happens for **9** and **10**. Both of these compounds exhibit one quadrupole-split doublet.

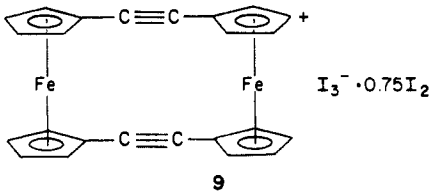

9

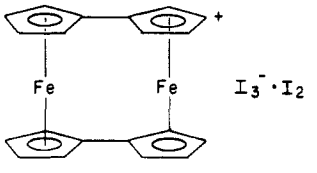

10

In the case of **9** ΔE_Q was reported to be 1.519 (5) mm/s at 300 K. The value of ΔE_Q at 300 K for **10** is even larger (1.719 (3) mm/s).[6] The cations in **9** and **10** are known[17] to have completely delocalized electronic structures based on IR data. That is, the strong electronic couplings in the cations of **9** and **10** lead to a situation where there is no potential energy barrier for intramolecular electron transfer.

Additional support for the statement that the intramolecular electronic coupling within the cations of **2** and **3** is not any greater than is present in the cation of **4** can be gleaned from the electrochemical data[10] for the three neutral unoxidized biferrocenes. Each shows two one-electron oxidation waves, and the two potentials for each of these three complexes are essentially identical from one complex to another. In fact, the separation between the two one-electron oxidation waves is the same for the unoxidized forms of the cations in **1**, **2**, **3**, and **4**.

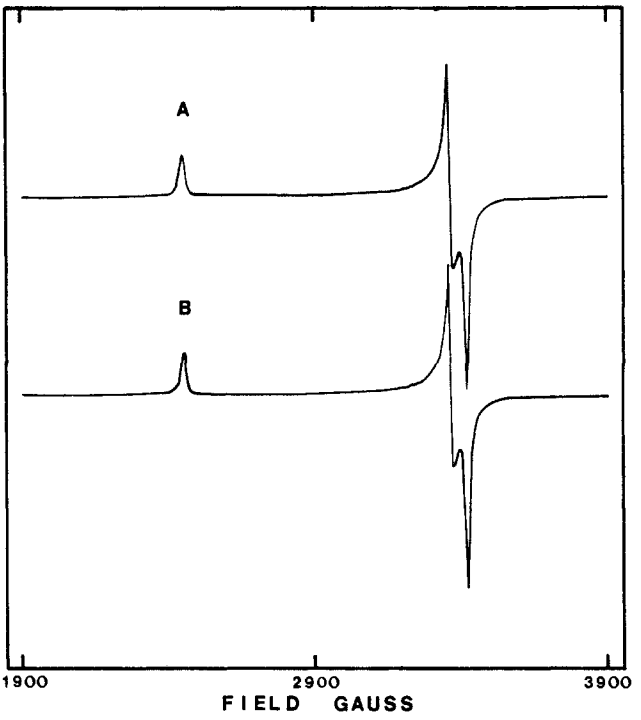

Figure 6. X-band EPR spectra at 4.2 K for microcrystalline samples of (A) 1′,6′-diiodobiferrocenium triiodide (**2**) and (B) 1′,6′-dibromobiferrocenium triiodide (**3**).

Table VIII. Electron Paramagnetic Resonance Data[a]

compd	T, K	$g_\parallel$	$g_\perp$	Δg^b
ferrocenium triiodide[c]	20	4.35	1.26	3.09
11[d]	12	4.00	1.92	2.08
12[d]	12	3.86	1.81	2.05
1[e]	12	3.58	1.72	1.86
1′-*n*-butylbiferrocenium triiodide	4.2	3.43	1.80	1.63
8[f]	4.2	3.42	1.84	1.58
4	4.2	3.28[g]	1.88[g]	1.40[g]
5	3.3	3.02	2.01	1.07
			1.89	
7[f]	4.2	2.98	1.92	1.06
3	4.2	2.76	2.01	0.78
			1.96	
2	4.2	2.75	2.01	0.76
			1.97	
9[h]	5.1	2.52	1.97	0.60
			1.88	
10[e]	12	2.36	1.99	0.41
			1.91	

[a] EPR spectra were run for microcrystalline samples. [b] This is the g-tensor anisotropy defined as $\Delta g = g_\parallel - g_\perp$. When a rhombic signal is seen, an average of two $g_\perp$ values is used for $g_\perp$. [c] Anderson, S. E.; Rai, R. *Chem. Phys.* **1973**, *2*, 216. Sohn, Y. S.; Henrickson, D. N.; Gray, H. B. *J. Am. Chem. Soc.* **1971**, *93*, 3603. [d] Rfeence 19. [e] Reference 5. [f] These samples were recrystallized by diffusion of hexane into a CH_2Cl_2 solution of the complex. [g] There is some uncertainity in these numbers as a result of broad spectral features. [h] Reference 17.

Electron Paramagnetic Resonance. X-band EPR spectra were run at liquid-helium temperatures for microcrystalline samples of **2**, **3**, **4**, **5**, **7**, **8**, and 1′-*n*-butylbiferrocenium triiodide. An "axial"-type spectrum was observed for the last three complexes. The spectrum obtained for **4** also looked to be axial: however, the signals are broad and additional broad but weak signals are present. In the cases of **2** and **3** "rhombic" EPR signals are seen, as illustrated in Figure 6. The *g* values extracted from all of these spectra are collected in Table VIII, together with some *g* values from the literature.

The $^2E_{2g}[(a_{1g})^2(e_{2g})^3]$ state of a *mononuclear* ferrocenium-type ion is split into two Kramers doublets [E″ and (A′, A″) in D_5

double groups] under the influence of spin–orbit coupling. Crystal fields of symmetry lower than D_5 mix these two Kramers doublets.

The approximate g-value expressions appropriate for the E'' ground state of a *mononuclear* ferrocenium-type complex have been reported[18] to be

$$g_z = g_{//} = 2 + 4k[-(\xi/\delta)/(1 + \xi^2/\delta^2)^{1/2}]$$

$$g_x = g_y = g_\perp = 2/(1 + \xi^2/\delta^2)^{1/2}$$

In these expressions, ξ is the spin-orbital coupling constant, k is the orbital-reduction factor, and δ is a one-electron splitting parameter gauging the effects of crystal fields lower in symmetry than D_5. For such a mononuclear Fe^{III} metallocene if there is no low-symmetry crystal field ($\delta = 0$) and k is unity, then $g_{//} = 6$ and $g_\perp = 0$. As the low-symmetry crystal field distortion increases, both $g_{//}$ and $g_\perp$ approach a value of 2. From Table VIII it can be seen that ferrocenium triiodide gives an axial 20 K EPR signal characterized by $g_{//} = 4.35$ and $g_\perp = 1.26$. The g-tensor anisotropy, $\Delta g = g_{//} - g_\perp$, is 3.09. The influence of substituents on the EPR signal has been studied[19] for a number of ferrocenium complexes such as **11** and **12**. The g-tensor anisotropy is reduced for **11** and **12** compared to salts of the unsubstituted ferrocenium

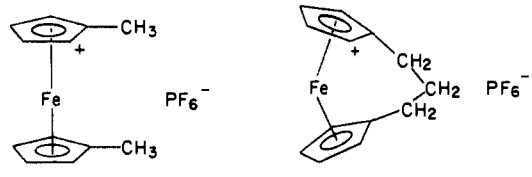

11 **12**

ion. In the case of **12** it is expected that the low-symmetry crystal-field distortion is quite large. The X-ray structure[20] of α-keto-1,1'-trimethyleneferrocene shows a ring tilt of 8.8°.

The g-tensor anisotropy (1.86) for **1** is even less than that for **12** (2.05). A further reduction is seen in the series **8** > **4** > **5** > **7**, where in the case of **7** $\Delta g = 1.06$. In the limiting case of the complexes **9** and **10**, Δg is 0.60 and 0.41, respectively. As indicated (vide supra and vide infra), complexes **9** and **10** have completely delocalized electronic structures as clearly indicated by their IR spectra. That is, they have no potential energy barriers for intramolecular electron transfer and, consequently, are delocalized on the EPR time scale. It is interesting that the Δg values for **2** (0.76) and **3** (0.78) suggest that the cations in these two compounds are also delocalized on the EPR time scale. If this is the case, then the rates of intramolecular electron transfer in **2** and **3** not only exceed $\sim 10^7$ s^{-1} (Mössbauer) but also exceed $\sim 10^9$–10^{10} s^{-1} from 300 down to 4.2 K. Additional evidence that **2** and **3** are delocalized on the EPR time scale is available from the temperature dependencies of the EPR signals. In the case of **2** and **3** EPR signals can be readily seen at room temperature. This is also the case for the delocalized species **9** and **10**. On the other hand, EPR signals for the other species in Table VIII are visible at low temperatures but cannot be seen at temperatures above ~200 K. In Figure 7 is shown the temperature dependence of the EPR spectrum for a microcrystalline sample of **5**, where it can be seen that the EPR spectrum for this compound becomes very broad by 180 K.

It is possible that *low*-temperature single-crystal EPR studies of, for example, complexes **1** and **2** could establish definitively whether or not **2** has an electron-transfer rate in excess of $\sim 10^9$–10^{10} s^{-1}. In these single-crystal EPR studies it would be

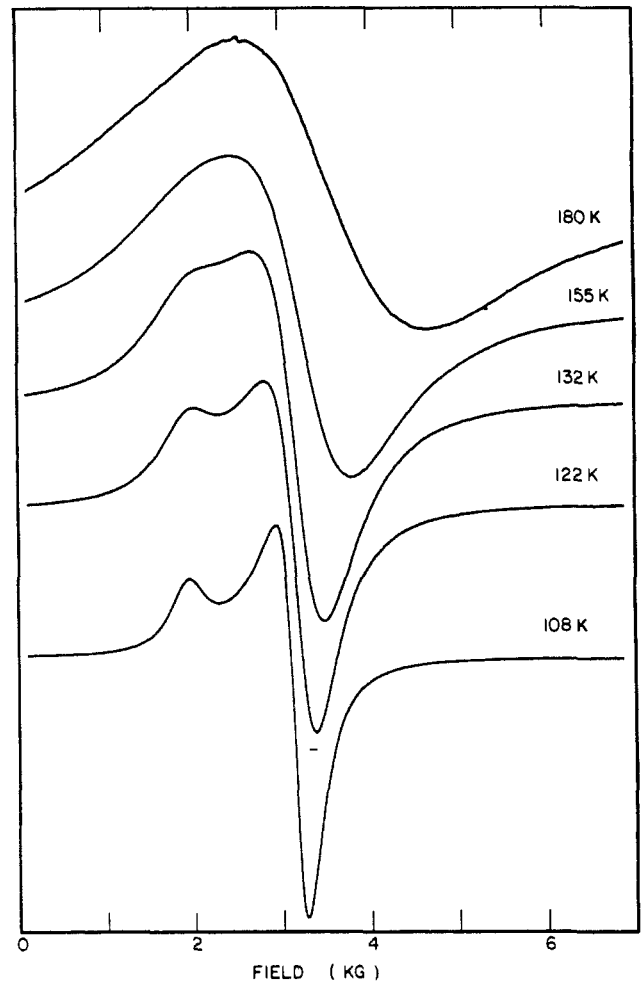

Figure 7. Variable-temperature X-band EPR spectra for a microcrystalline sample of 1',6'-diethylbiferrocenium triiodide.

expected that, as a result of a relatively localized electronic structure, the magnetic z axis for the cation in **1** would be directed along the pseudo-C_5 axis of a metallocene moiety, whereas for **2**, the magnetic z axis could be along the Fe···Fe direction of the cation.

Infrared Spectroscopy. If the cations in **2** and **3** are delocalized on the ^{57}Fe Mössbauer and EPR time scales, the immediate question is whether there is or is not a potential energy barrier for electron transfer in these species. IR spectroscopy has proven to be useful in making this assessment.[17] When an Fe^{II} metallocene is oxidized to an Fe^{III} metallocene, there is a dramatic change in the IR spectrum. It has been shown[17] that the perpendicular C–H bending band is most diagnostic of the oxidation state. This band is seen at 815 cm^{-1} for ferrocene and at 851 cm^{-1} for ferrocenium triiodide. The cation in **9** is delocalized (i.e., no barrier) because there is only one band at 830 cm^{-1}. A mixed-valence cation that does have a barrier shows both Fe^{II} and Fe^{III} perpendicular C–H bending bands.

Variable-temperature (50–300 K) FTIR spectra were run for KBr pellets of **2**, **3**, and **4**. In Figure 8 are illustrated the 50 and 298 K spectra of **3** and the 300 K spectrum (trace A) of unoxidized 1',6'-dibromobiferrocene. In the perpendicular C–H bending region there is a strong band at 822 cm^{-1} with a shoulder at 815 cm^{-1} in the 300 K spectrum (trace A) of 1',6'-dibromobiferrocene. The mixed-valence compound **3** shows relatively strong bands at 822 and 849 cm^{-1} at 298 K. It is clear that on the IR time scale ($\sim 10^{-11}$–10^{-12} s) the mixed-valence cation in **3** has both Fe^{II} and Fe^{III} moieties. As is evident in Figure 8, there is little temperature dependence seen in the IR spectrum of **3** in the 300–50 K range.

The uncertainty principle ($\Delta t \Delta \nu \sim {}^1/_{2\pi}$) can be used to establish an upper limit on the rate of electron transfer in **3**, and for that matter in **2** and **4**. The Fe^{II} and Fe^{III} C–H bending bands

(14) Mammano, N. J.; Zalkin, A.; Landers, A.; Rheingold, A. L. *Inorg. Chem.* **1977**, *16*, 297.
(15) Seiler, P.; Dunitz, J. D. *Acta Crystallogr., Sect. B* **1979**, *35*, 1065.
(16) Runsink, J.; Swen-Walstra, S.; Migchelsen, T. *Acta Crystallogr., Sect. B* **1972**, *28*, 1331.
(17) Kramer, J. A.; Hendrickson, D. N. *Inorg. Chem.* **1980**, *19*, 3330.
(18) (a) Prins, R.; Kortbeek, A. *J. Organomet. Chem.* **1971**, *33*, C33; (b) Hendrickson, D. N.; Sohn, Y. S.; Gray, H. B. *Inorg. Chem.* **1971**, *10*, 1559.
(19) Duggan, D. M.; Hendrickson, D. N. *Inorg. Chem.* **1975**, *14*, 955.
(20) Jones, N. D.; Marsh, R. E.; Richards, J. H. *Acta Crystallogr.* **1965**, *19*, 330.

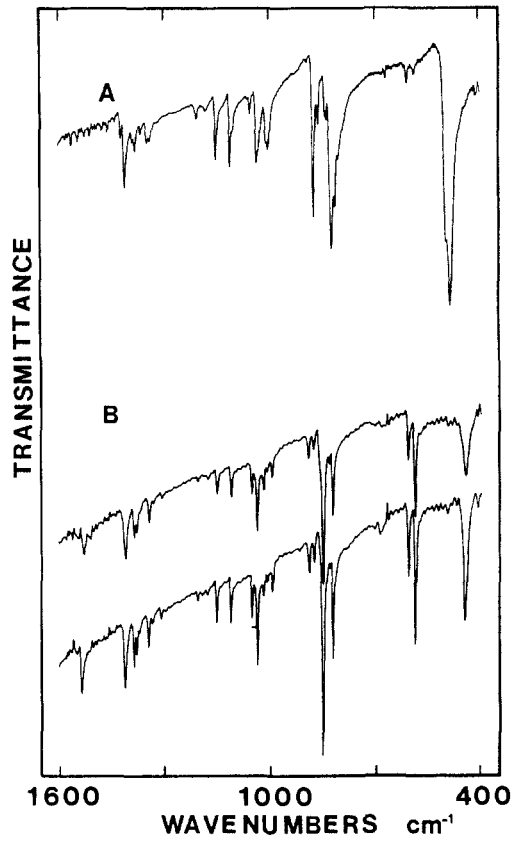

Figure 8. FTIR spectra of KBr pellets of (A) 1′,6′-dibromobiferrocene at 298 K and (B) 1′,6′-dibromobiferrocenium triiodide at 298 K (upper trace) and 50 K (lower trace).

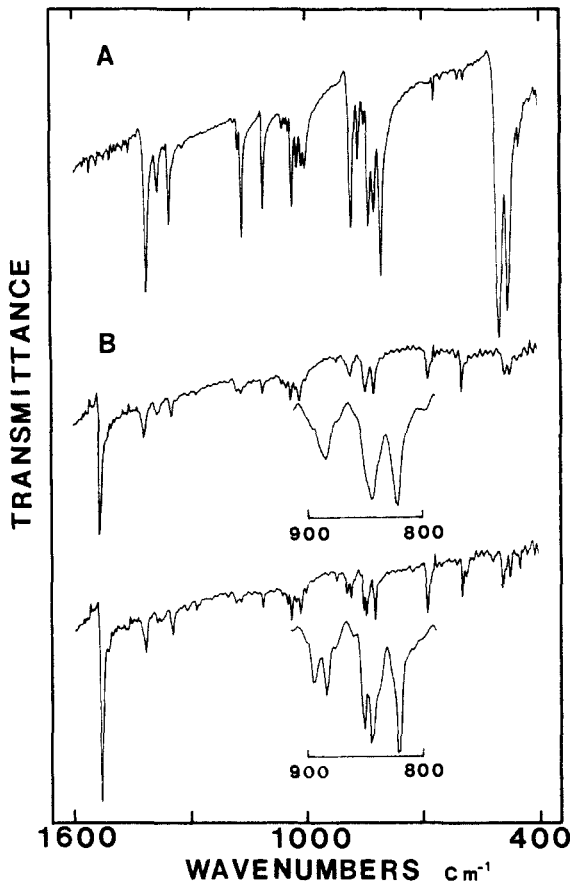

Figure 9. FTIR spectra of KBr pellets of (A) 1′,6′-dichlorobiferrocene at 298 K and (B) 1′,6′-dichlorobiferrocenium triiodide at 298 K (upper trace) and 50 K (lower trace). Insets show expanded views of the perpendicular C–H bending region.

do *not* seem to have line widths that are appreciably different than other bands in the spectra. The rate of electron transfer is slower than would lead to a broadening of these bands. The line widths of these bands are on the order of 5 cm^{-1}, and this gives an estimate of $\Delta\nu$. As a consequence, the rate of electron transfer is slower than 2.4×10^{10} s^{-1} ($=\Delta\nu/2\pi$).

The IR spectra of **2** look very similar to those illustrated in Figure 8 for **3** (a figure showing the spectra for **2** is available in the supplementary material). Mixed-valence complex **2** shows perpendicular C–H bending bands at 820 and 834 cm^{-1} at 298 K. It also has Fe^{II} and Fe^{III} moieties.

Illustrated in Figure 9 are IR spectra for **4** and for 1′,6′-dichlorobiferrocene, the latter of which shows at 300 K a strong band at 804 cm^{-1} and a lower intensity bands at 822 and 835 cm^{-1} in the perpendicular C–H bending region. The mixed-valence complex **4** shows two bands at 822 and 845 cm^{-1} in the 298 K spectrum. It appears that the higher energy band is resolved into two bands (845 and 851 cm^{-1}) in the 50 K spectrum. Thus, the spectra for **4** again indicate the presence of Fe^{II} and Fe^{III} moieties, which is necessitated by the Mössbauer data for this complex.

Effect of Environment on Intramolecular Electron-Transfer Rate. The Mössbauer and EPR results clearly indicate that the *intra*molecular electron-transfer rate in **4** is less than $\sim 10^7$ s^{-1}, whereas, the rate for **2** and **3** is greater than $\sim 10^9$–10^{10} s^{-1}. This difference does not grow out of a difference in electronic or vibronic coupling in the series **2**, **3**, and **4**. The X-ray structure of **4** does show that the environment about the 1′,6′-dichlorobiferrocenium cation is not symmetric, that is, the two iron ions are not in equivalent environments. This asymmetry in the environment increases the potential-energy barrier for intramolecular electron transfer. One vibronic state of the mixed-valence cation, i.e., $Fe_a^{III}Fe_b^{II}$, is energetically more stable than the other state $Fe_a^{II}Fe_b^{III}$.

In the case of **2**, and presumably **3**, the environment about the mixed-valence cation in the solid state is identical for the two iron ions in the cation. There is no zero-point energy difference between the two vibronic states and the rate of *intra*molecular electron transfer is much greater for the cations in **2** and **3** than for the cation in **4**. The influence of the solid-state environment on the rate of intramolecular electron transfer appears to be quite pronounced in these mixed-valence complexes. In the case of mixed-valence cations the placement and nature of the anions is crucial. In a recent communication[3] and forthcoming publications[21] it has been demonstrated that large changes in the temperature at which the mixed-valence biferrocene transfers electrons faster than the Mössbauer time scale can be effected by simply replacing I_3^- by Br–I–Br^-, which is also linear and ~7% shorter than I_3^-. For example, in the case of compound **1** replacing the I_3^- anion by Br_2I^- leads to a change from ~350 to ~200 K in the temperature at which the biferrocenium cation transfers electron more rapidly than the Mössbauer technique can sense.[3]

Similar dramatic effects of solid-state environment controlling the rate of *intra*molecular electron transfer have been noted[22-24] for several mixed-valence oxo-centered iron acetate complexes of the composition $[Fe_3O(O_2CCH_3)_6(X\text{-}py)_3]S$, where S is some solvate molecule such as benzene and X-py is a substituted pyridine. It has been found that dynamics in the solid state involving the onset of motion in a ligand and/or solvate molecule at a certain temperature is a major factor determining whether the *intra*molecular electron transfer in a given mixed-valence complex is fast or slow. Evidence for this is now available from heat capacity[23,25] and solid-state ^2H NMR[23,26] studies. An ov-

(21) Dong, T.-Y.; Hendrickson, D. N., manuscript in preparation.
(22) Oh, S. M.; Hendrickson, D. N.; Hassett, K. L.; Davis, R. E. *J. Am. Chem. Soc.* **1984**, *106*, 7984.
(23) Oh, S. M.; Kambara, T.; Hendrickson, D. N.; Sorai, M.; Kaji, K.; Woehler, S. E.; Wittebort, R. J. *J. Am. Chem. Soc.* **1985**, *107*, 5540.
(24) Oh, S. M.; Hendrickson, D. N.; Hassett, K. L.; Davis, R. E. *J. Am. Chem. Soc.* **1985**, *107*, 8009.
(25) Sorai, M.; Kaji, K.; Hendrickson, D. N.; Oh, S. M. *J. Am. Chem. Soc.*, in press.
(26) Woehler, S. E.; Wittebort, R. J.; Oh, S. M.; Hendrickson, D. N.; Strouse, C. E., to be submitted.

erview of research progress in this area is available.[27]

Finally, it should be noted that it is amazing that the rate of *intra*molecular electron transfer for the mixed-valence cations in **2** and **3** is greater than $\sim 10^{10}$ s^{-1} (or even $\sim 10^{7}$ s^{-1}) at 4.2 K. Obviously, there is no thermal energy available at this temperature. The infrared spectra for these two compounds indicate that there is a potential energy barrier for electron transfer. The inescapable conclusion is that the *intra*molecular electron transfer in **2** and **3** at temperatures in the liquid-helium temperature range proceeds by an electron and nuclear tunneling mechanism. If this is the case, there is a reasonably good probability that a large fraction of the electron transferring at room temperature also proceeds by a tunneling mechanism.

(27) Hendrickson, D. N.; Oh, S. M.; Dong, T.-Y.; Moore, M. F. *Comments Inorg. Chem.*, in press.

Acknowledgment. We are grateful for support from National Institutes of Health Grant HL13652 (to D.N.H.).

Registry No. 2, 56030-43-4; **3**, 88005-31-6; **4**, 88005-33-8.

Supplementary Material Available: Observed and calculated structure factors and thermal parameters for compounds **2** and **4**; figure showing the infrared spectra for **2** at 298 and 50 K and for 1′,6′-diiodobiferrocene at 298 K (14 pages). Ordering information is given on any current masthead page.

A Series of Edge-Sharing Bioctahedral, M–M Bonded Molecules: Non-Monotonic Bond Length Variation and Its Interpretation

Akhil R. Chakravarty, F. Albert Cotton,* Michael P. Diebold, Diane B. Lewis, and Wieslaw J. Roth

Contribution from the Department of Chemistry and Laboratory for Molecular Structure and Bonding, Texas A&M University, College Station, Texas 77843. *Received August 2, 1985*

Abstract: Three new stoichiometrically homologous compounds, $Ta_2Cl_6(dmpm)_2$ (**1**), $Mo_2Cl_6(dppm)_2$ (**2**), and $Ru_2Cl_6(dmpm)_2$ (**3**), have been prepared and their structures determined. Crystal data are as follows. **1**: $P2_1/n$, $a = 7.263$ (3) Å, $b = 15.536$ (3) Å, $c = 10.827$ (2) Å, $\beta = 93.73$ (2)°, $V = 1219$ (1) Å^3, $Z = 2$. **2**: $C2/c$, $a = 23.083$ (4) Å, $b = 10.866$ (4) Å, $c = 23.254$ (5) Å, $\beta = 124.25$ (3)°, $V = 4821$ (4) Å^3, $Z = 4$. **3**: $I2/a$, $a = 12.479$ (5) Å, $b = 15.330$ (6) Å, $c = 13.212$ (4) Å, $\beta = 113.91$ (3)°, $V = 2310$ (1) Å^3, $Z = 4$. These three compounds, as well as the previously described $Nb_2Cl_6(dmpm)_2$ and $Re_2Cl_6(dppm)_2$, consist of molecules in which two octahedra share an edge via μ-Cl atoms, thus forming a central, planar $Cl_2M(\mu\text{-}Cl)_2MCl_2$ unit with bridging dmpm or dppm molecules connecting pairs of adjacent axial positions above and below the central plane. The M–M distances in these five molecules are the following: Nb–Nb, 2.711 (3) Å; Ta–Ta, 2.692 (2) Å; Mo–Mo, 2.789 (1) Å; Re–Re, 2.616 (1) Å; Ru–Ru, 2.933 (1) Å. The up, down, up variation on proceeding through the d^2–d^2, d^3–d^3, d^4–d^4, d^5–d^5 series of metal atom pairs is consistent with the following electronic configurations: $\sigma^2\pi^2$, $\sigma^2\pi^2\delta^{*2}$, $\sigma^2\pi^2\delta^{*2}\delta^2$, $\sigma^2\pi^2\delta^{*2}\delta^2\pi^{*2}$. The relationship of this structurally indicated ordering of the orbitals is discussed in the light of molecular quantum mechanical calculations on model systems, and it is shown that the overall experimental and theoretical picture is internally consistent.

The juxtaposition of two metal atoms in the edge-sharing bioctahedron type of structure I affords the opportunity to study metal–metal (M–M) bonding under conditions that are, in principle, under control yet widely variable. The situation is not only inherently interesting but relevent to M–M interactions that are of importance, but less amenable to systematic study, in solid-state chemistry.

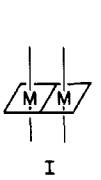

I

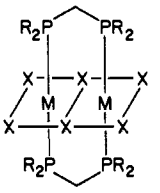

II

R = CH_3, C_6H_5
X = Cl

Before the *potentially* available opportunities to study systematically such complexes can actually be exploited, synthetic methods are required that allow us to make, by design, species whose behavior is expected to be interesting. In this laboratory we are developing such synthetic methods and a few reports have already appeared.[1-3] We have also conducted several studies of of the M–M bonding in these complexes using structural and magnetic data as well as molecular orbital calculations.[1-4] Further synthetic work and spectroscopic studies are also in hand and will be reported shortly along with pertinent structural and magnetic data.

For a particular series of structurally homologous compounds, namely those for which the general representation is II, with R = CH_3 or Ph, and the metal atoms are from groups V, VI, VII, and VIII, we now have data that allow us to provide what we believe is direct evidence for the ordering of the molecular orbitals responsible for M–M bonding in this general type of interaction. We have previously reported the compounds of the type II in which M = Nb[2] and Re.[1] We now have the compounds with M = Ta, Mo, and Ru. A comparison of the first of these with the niobium compound shows that the differences (at least structural ones) caused by changing from a second transition series metal to its congener in the third transition series, or vice versa, are not critical.

(1) Barder, T. J.; Cotton, F. A.; Lewis, D.; Schwotzer, W.; Tetrick, S. M.; Walton, R. A. *J. Am. Chem. Soc.* **1984**, *106*, 2882.
(2) Cotton, F. A.; Duraj, S. A.; Falvello, L. R.; Roth, W. J. *Inorg. Chem.* **1985**, *24*, 4389.
(3) Cotton, F. A.; Diebold, M. P.; O'Conner, C. J.; Powell, G. L. *J. Am. Chem. Soc.* **1985**, *107*, 7438.
(4) Anderson, L. B.; Cotton, F. A.; DeMarco, D.; Fang, A.; Ilsley, W. H.; Kolthammer, B. W. S.; Walton, R. A. *J. Am. Chem. Soc.* **1981**, *103*, 5078.

0002-7863/86/1508-0971$01.50/0